

## Modelling of transport phenomena and defects in crystal growth processes

S PENDURTI, H ZHANG and V PRASAD

Consortium for Crystal Growth Research, Department of Mechanical Engineering, State University of New York at Stony Brook, Stony Brook, NY 11794-2300, USA  
e-mail: vprasad@notes.cc.sunysb.edu

**Abstract.** A brief review of single crystal growth techniques and the associated problems is presented. Emphasis is placed on models for various transport and defect phenomena involved in the growth process with the ultimate aim of integrating them into a comprehensive numerical model. The sources of dislocation nucleation in the growing crystal are discussed, and the propagation and multiplication of these under the action of thermal stresses is discussed. A brief description of a high-level numerical technique based on multiple adaptive grid generation and finite volume discretization is presented, followed by the result of a representative numerical simulation.

**Keywords.** Transport phenomena; crystal growth defects; thermal stresses; multiple adaptive grid generation; finite volume discretization.

### 1. Introduction

Semiconductor materials have become the most important and characteristic materials of the information age. Elemental semiconductors like Si, Ge, and compound III–V semiconductors like InP, GaAs, form the heart of the semiconductor industry. They are used for crucial electronic and communication applications, as well as for a variety of many other high technology devices and system. Though silicon-based technology accounts for more than 90% of the current semiconductor market, in recent years, the availability of bulk single crystals of InP and GaAs has opened the avenues for new, exciting applications of these materials. They are playing an increasingly important role in microwave devices, millimeterwave devices, circuit technology, photovoltaic applications, opto-electronics, and photonics. In the area of opto-electronics, the development of low-loss optical fibres, with optimum characteristics in the 1.1 to 1.6  $\mu\text{m}$  wavelength region, has led to the development of InP-based devices which work in the same wavelength. Thus, these devices are being used widely in optical fibre communications all over the world, and are the primary components of the burgeoning information superhighway. GaAs has attractive photovoltaic (PV) properties, and its surface is readily passivated with wide bandgap, lattice-matched layers. Its bandgap is nearly optimum for the solar spectrum. In the field of

photonics, N-type GaAs substrates are extensively utilized in high power lasers emitting at 0.87  $\mu\text{m}$  and light-emitting diodes (LEDs).

In recent years, the trend towards greater bandwidth requires a shift from solid-state infrared lasers to visible blue light laser, which can operate at room temperature and above. Correspondingly, substrate technology is moving to growing crystals of gallium nitride (GaN) and zinc oxide (ZnO), which involves formidable technological challenges. A new exciting material is SiC, which has very attractive properties. It is a wide bandgap semiconductor with physical and electronic properties unmatched for high-temperature, high-frequency, and high-power electronic device application. II-VI semiconductors such as CdTe are being used as substrate materials for blue laser, LEDs, and also for a number of devices used for the detection of infrared, X-ray, and gamma radiations. Thus, semiconductor technology, though still dominated by Si, poses the demand for newer and more specialized materials – GaAs, Inp, GaN, CdTe, SiC etc. – the manufacture of which involves increasing degrees of complexity.

Thus the aim of crystal growers is not only to perfect crystal growth techniques for existing materials, but also to extend them to new ones. The advent of computers has given them a new tool to deal with the problem – numerical modelling. The aim of this paper is to present a brief review of the important basic phenomena, associated with crystal growth techniques involving solidification from the melt, and their integration into a numerical model. Special emphasis has been placed on transport phenomena, defects, and the techniques to deal with the solidification interface. Accordingly, a brief review of the basic growth techniques is given in § 2, followed by a discussion of some pressing issues in § 3. Section 4 presents various theoretical formulations for the transport phenomena involved, and a brief description of the numerical strategy adopted by the present authors and their co-workers. Section 5 discusses theoretical models for defect formation in as-grown crystals, and lastly in § 6, a representative numerical simulation is presented, to illustrate both the power and limitations of the modelling efforts so far.

## 2. Growth techniques

The bulk of modern day requirements of Si and III-V's are met by techniques involving pulling single crystals from their melt – Czochralski and its variants, Bridgman and its variations, float zone melting etc. Fundamentally, all the techniques which involve growth of single crystals through solidification from a melt can be broadly classified as confined and meniscus-defined growth techniques (Brown 1988). Examples of the former are the vertical Bridgman method, and the gradient freeze method, where the material is loaded into an ampoule, melted and resolidified, by either varying heater power (gradient freeze method), or translating the ampoule (vertical Bridgman method). In meniscus-defined crystal growth techniques, such as Czochralski (Cz), liquid-encapsulated Cz (LEC), and floating zone, a seed crystal is dipped into a pool of melt and the thermal environment is varied such that the melt solidifies on the seed, which is then pulled as a single crystal, while the solidification proceeds. A brief description of the two most common techniques, Czochralski and Bridgman methods, is as follows.

### 2.1 Czochralski technique

The Czochralski process is the most popular technique for growing single crystals, and almost all Si single crystals for electronic devices are grown using this method. The

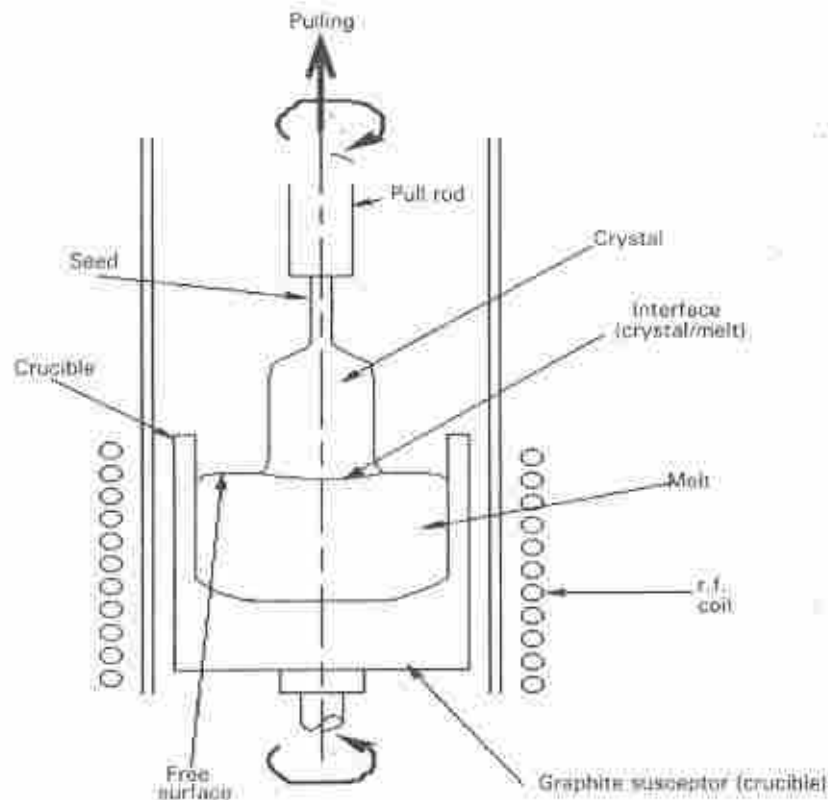


Figure 1. Schematic of a low pressure Czochralski system.

technique was developed as a result of the pioneering work by Czochralski (1917), and was later perfected by Teal & Little (1950), who adapted this technique to the growth of single crystals. They introduced provision for careful control of the heating power supplied, and introduced the concept of rotation of the crystal as it is being pulled from the melt, which are now instrumental for features like diameter control, radial symmetry of the thermal distribution, and also radial uniformity of the distribution of the dopants. The technique basically consists of a rotating crucible, refer figure 1, which contains the charge material to be crystallized surrounded by a heater capable of melting the charge and maintaining it in a molten condition. A pull rod, with a seed crystal attached to its bottom and rotating usually in a direction opposite to that of the crucible, is mounted coaxially, and lowered until the end of the seed touches the melt. The melt temperature is carefully adjusted until a meniscus is supported by the end of the seed. Once a thermal steady state is achieved, the pull rod is carefully rotated and lifted, while the melt crystallizes on the seed. The diameter of the crystal is increased from that of the seed to a desired value, by careful variation of the heater power and pulling rate. The crystal and the crucible are rotated during the whole process to maintain radial homogeneity. The whole crystal growth assembly is placed in a closed water-cooled chamber, which is evacuated and filled with an inert gas (generally argon) at a low pressure, this is to ensure that the system is shielded from the effect of harmful atmospheric gases and temperature fluctuations of the ambient. The pulling rates vary according to size of the crystal desired, the material and other considerations.

Typically, for Si growth, they are of the order of 0.1 m/h, while for III-V materials, they are of the order of 0.01 m/h.

For III-V compounds the technique is more complicated owing to the dissociability of the melt of these materials. For example, a GaAs melt can dissociate into Ga and As, resulting in bubbles of arsenic vapour escaping from the melt. This can affect the stoichiometry of the melt.

The problem of decomposition has been overcome through a novel modification – the LEC technique, figure 2. If high pressure is not required to maintain the chemical equilibrium (i.e., the vapour pressure of the volatile component is not high), only minor modifications of the standard Czochralski system are required. In the case of GaAs, for example, it involves charging the crucible with a quantity of boric oxide, a low-melting point glass, in addition to the polycrystalline gallium arsenide. On heating the crucible, the boric oxide softens and flows over the charge. Since it wets the crucible, and is immiscible with and lighter than the melt, it encapsulates the charge. An inert gas is introduced into the growth chamber, at a pressure higher than the dissociation pressure of the GaAs melt, preventing loss of As from the melt surface. This suppresses the arsenic-bubble formation. Being essentially insoluble in boric oxide, arsenic cannot diffuse through it. Crystal growing is performed in the usual manner by lowering the seed crystal through the encapsulant layer, until it contacts the melt interface; pulling is then initiated in the usual way.

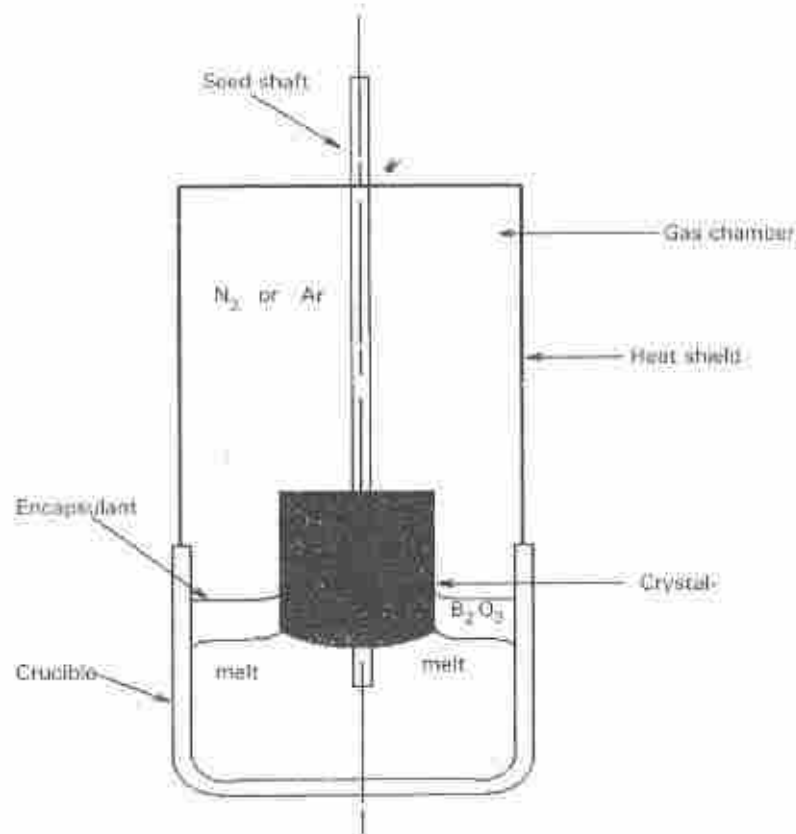


Figure 2. Schematic of a high pressure liquid-encapsulated Czochralski system.

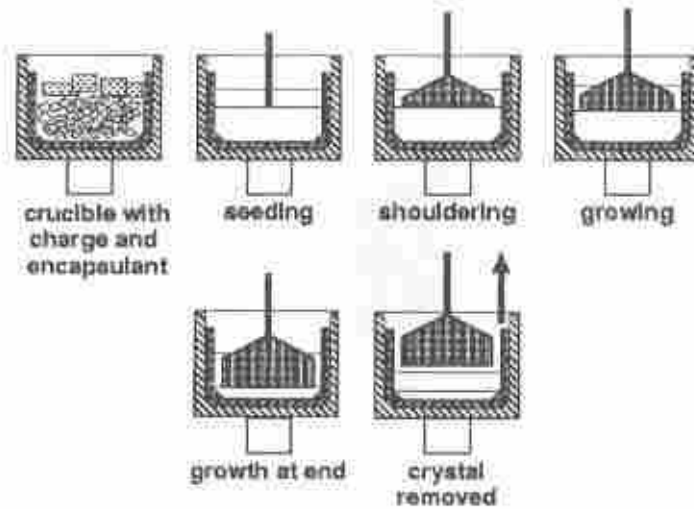


Figure 3. Various steps in a liquid-encapsulated Cz (LEC) process.

Figure 3 shows the schematic of the growth process for high pressure III–V compounds growth. The pressure of the inert gas in the growth chamber depends on the dissociation pressure of the melt and may range from about 1 atm\* for GaAs, through 40 atm for InP, to 70 atm for compounds like GaP, and much higher pressures for GaN, ZnO etc. The complexity and technological challenges associated with the LEC technique increase greatly with the pressure, and for this reason GaAs is still one of the easiest III–V materials to grow.

## 2.2 Bridgman and gradient freeze techniques

In these techniques, the basic process is of loading a polycrystalline charge of the material into a crucible containing a single crystal seed at the bottom. The crucible is then heated in a furnace, till the polycrystalline charge and a part of the single crystal seed are melted. The temperature field in the crucible is then adjusted until solidification starts at the seed and proceeds till the whole of the melted charge has solidified as a single crystal. The temperature field has to be continuously adjusted, so that the freezing point isotherm always corresponds with the interface as the solidification proceeds.

If this is done by traversing the crucible through the furnace, the term Bridgman or Bridgman–Stockbarger is applied. However, if the temperature field is made to move across the charge, by ramping the power supplied to a single zone furnace, or by adjusting the power supply in an array of furnaces, then the terms gradient freeze or dynamic gradient freeze are used. The vertical configuration of the gradient-freeze technique is illustrated in figure 4. A more sophisticated version of this method is the electro-dynamic gradient freeze (EDGF) in which the furnace is composed of 20–50 independently controlled heating zones. In the case of III–V materials, the melt is prone to dissociation and the group V element escapes as vapour. The variations made to overcome this add the prefix ‘modified’ to each of the techniques described in the preceding paragraph. A means

\*1 atm =  $1.01325 \times 10^5$  Pa

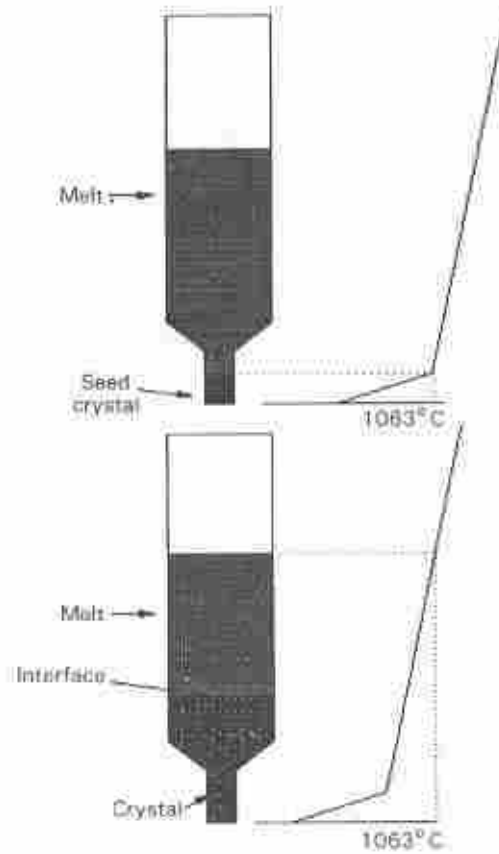


**Figure 4.** Schematic illustrating the adjustment of temperature field, as solidification proceeds, by ramping the power in a vertical gradient freeze technique. The melting point of InP is 1063°C.

of preventing this dissociation is to fill the system with the gas of the volatile component at a pressure above the dissociation pressure of the III-V compound or by the boric oxide layer encapsulation, as discussed in the case of the Czochralski method. The advantages of these methods, as opposed to the Czochralski technique is that the temperature field in these crystals can be closely controlled. They are characterized by relatively uniform radial, and axial distribution of dopants, low temperature gradients, and consequently, low dislocation and other defect densities. Thus single crystals with high structural perfection can be achieved. However, single crystals of only small diameters can be grown using this technique, thereby restricting its widespread commercial use. On the other hand, for a number of materials like II-VI compounds, certain oxides etc., the vertical gradient freeze technique or one of its variations is often the only method available.

### 3. Issues in crystal growth from the melt

The spectacular growth of the semiconductor technology has given rise to the need for high quality, large size single crystals. More specifically, the crystals grown need to have high structural perfection – absence of dislocations (line defects), point defects etc., and uniform

radial and axial distribution of the dopants. Apart from growing crystals of high quality, attention needs to be paid to issues like economy of the process, production rate, reproducibility of the process etc. Since large wafers mean substantial savings in device production, there is a continuous trend to upscale the crystal growth processes. Presently, commercial Si single crystals of diameter 200 mm and those of GaAs of around 100 mm are being produced. Though the techniques of Czochralski and VGF have been in vogue for at least fifty years, and these techniques have been applied to grow a large variety of materials, the actual growth process is still mostly an art.

The challenge before crystal growers is to devise schemes to tailor the microscopic properties of the growing crystal, by controlling a few macroscopic variables of the growth process, like heater power, pulling rates, rotation rates, applied magnetic fields etc. This task is particularly daunting because of the incredibly rich and diverse range of physical phenomena all interacting with one another, giving rise to an almost intractable nonlinear system. Often, the physics behind certain phenomena is unknown. For example, the generation of dislocations in the crystal has long been understood to be due to thermal gradients in the crystal, though the exact mechanism of defect formation, propagation and multiplication are yet unknown. Phenomenological models, elaborated in later sections, do exist, but these are rather unsatisfactory and suffer from several shortcomings. Another problem is the diverse timescales associated with various phenomena. For example, the striations of dopants found in crystals are believed to be due to micro-segregation, caused by random oscillations of the crystal/melt interface due to the inherently oscillatory and/or turbulent nature of the flow and non-equilibrium kinetics. To capture these phenomena in a crystal growth model, temporal resolution of the order of  $10^{-3}$  seconds is necessary, while the general growth process is a matter of hours and sometimes days. The reconciliation of these diverse timescales is still a matter of advanced research and is one of the major roadblocks to a complete simulation of the growth process. Figure 5 shows the interrelation between the diverse physical processes, their interactions and the relationship with the microstructural imperfections in the crystal. Thus there are many physical and engineering issues, which need to be addressed to improve scientific understanding of the growth phenomena. A brief description of the issues is given below.

*Complex flow:* The melt flow in a Cz or a VGF system is three-dimensionally oscillatory, and in many cases turbulent. This results in oscillations of the melt/crystal interface, and remelting/solidification, with corresponding fluctuations in the growth rate. The melt flow in the CZ system is primarily driven by a combination of the following modes of convection (Kobayashi 1978; Langlois 1981; Jones 1983; Hurle & Cockayne 1994), shown in figure 6. (1) Natural convection due to buoyancy forces produced by complex thermal boundary conditions, which include heating on the side walls, radiative cooling at the free surface and phase change at the crystal-melt interface, (2) Marangoni convection due to variation in surface tension with temperature and dopant concentration, (3) forced convection due to crystal and crucible rotations, and (4) forced convection due to crystal pulling as well as reduction in melt height. In the case of high pressure LEC growth, convection in the gas plays an important role in heat transfer in the system, and for this reason, computer simulations of the high pressure system are expected to be much more computationally intensive.

*Radiation:* Since crystal growth phenomena takes place at high temperatures, which often exceed  $1000^{\circ}\text{C}$ , the radiative mode of heat transfer is significant. Incorporation of this mode of

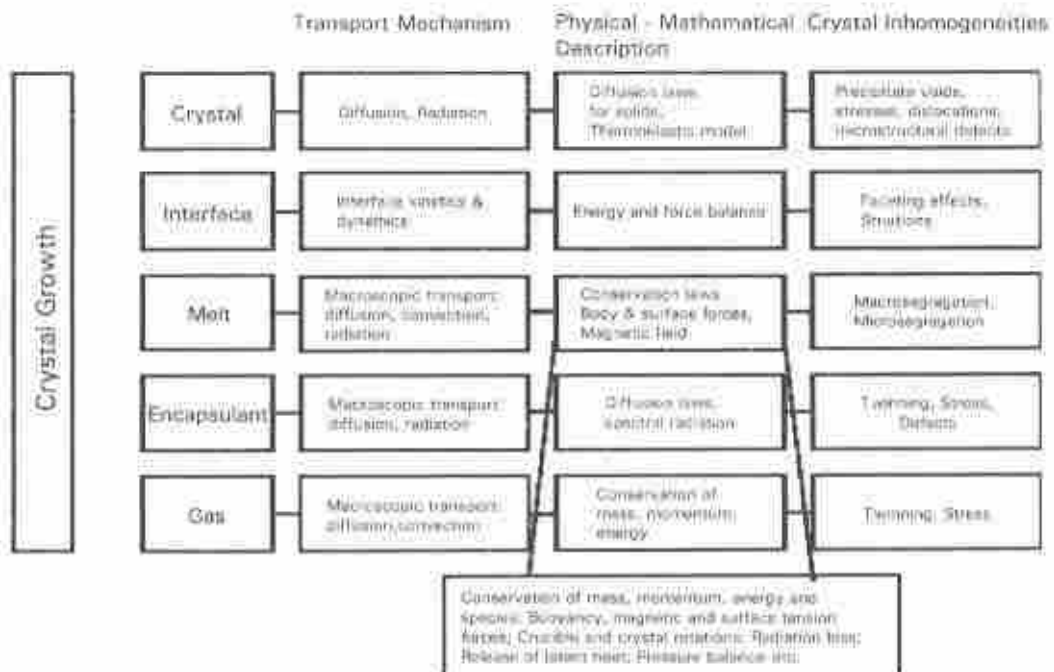


Figure 5. Various phenomena involved in crystal growth, and their interactions leading to the final quality of the crystal.

heat transfer into modelling efforts has not been easy due to the lack of concrete physical data. For example, very little is known about the radiative properties of the crystal. While some authors consider the crystal as fully transparent to all wavelengths (Atherton *et al* 1987), others approximate the crystal as opaque and transparent only to certain wavelengths (Nunes *et al* 1996). Radiation is more dominant in low pressure Czochralski growth of Si and other elemental semiconductors, due to the absence of gas convection in these systems.

**Segregation:** Segregation refers to the uneven distribution of the dopant in the crystal. This is one of the most critical issues in semiconductors, for instance in electronic or optoelectronic applications, the quality of the wafer is dependent on its chemical homogeneity. Segregation is due to the segregation coefficient varying from unity, leading to the solid rejecting or absorbing extra dopant, and thus leading to either accumulation or depletion of dopant in the melt. As a consequence, dopant concentration varies along the growth direction. Complex convection patterns in the melt complicate dopant distribution in the melt, leading to inhomogeneities in the axial as well as the radial directions of the crystal. Solute segregation at the microscopic level is termed as microsegregation and shows up in the form of striations in crystals. It is due to time-dependent variations in interface kinetics and growth velocity, which may be caused by temperature and flow fluctuations, non-equilibrium phenomena, or other equipment imperfections like pulling device instabilities, vibration in the equipment etc.

**Defects:** These are imperfections in the crystal lattice, and vary from material to material. In the case of III-V materials like GaAs and InP, the main defects are line defects, also

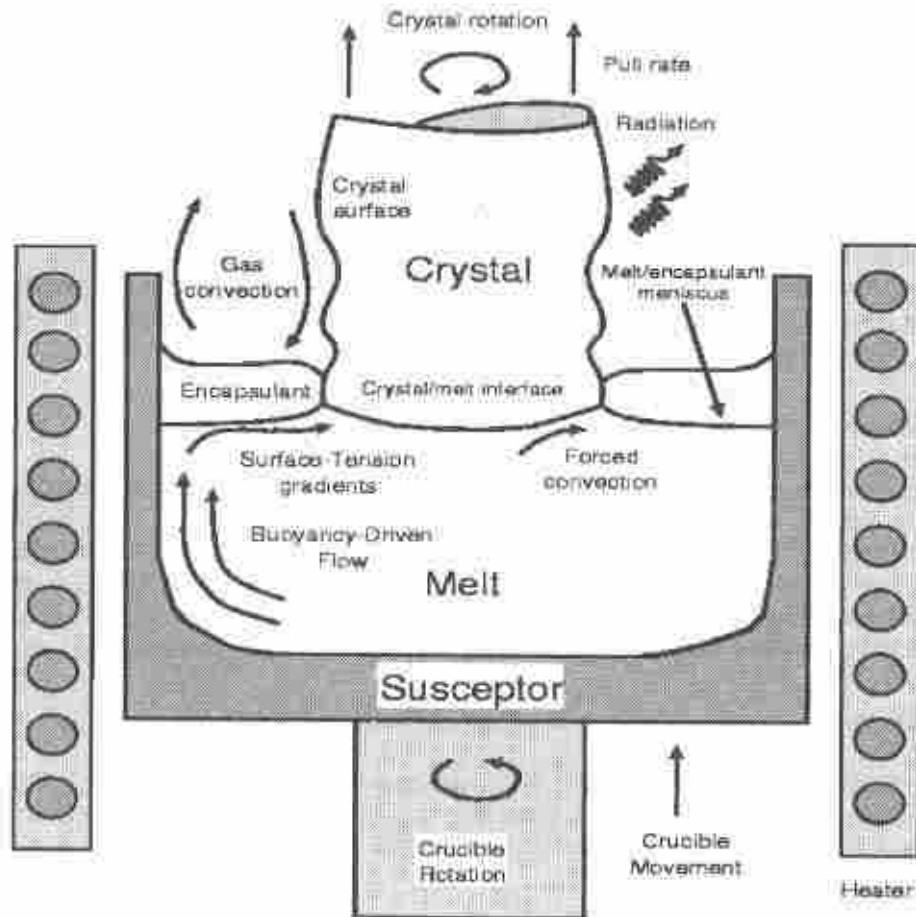


Figure 6. A schematic of the modes of heat transfer in the Czochralski system.

known as dislocations. The main cause of these is believed to be the thermal stress that arises due to a non-uniform temperature field in the crystal during growth. The crystal relieves the thermal stress through plastic deformation, by the movement and multiplication of dislocations. As will be discussed later, dislocations have major impact on the performance of electronic devices, and their elimination is the topic of major research. Following Dash's (1958) path-breaking work in the fifties, Si single crystals can now be grown dislocation-free, using the Czochralski technique. The main defects in Si are accumulations of point defects, some of which arise from fluctuations at the interface. One of the major considerations in LEC growth of InP is twinning. Twinning is prevalent in InP because of the low stacking-fault energy of this material, and this phenomenon has also been sometimes linked to oscillations in the crystal/melt interface.

*Use of magnetic field:* A magnetic field can stabilize the interface condition to some extent, but is expensive and its effect on melt conditions is not well understood. Also, the materials for which the use of magnets can be commercially justified and conditions under which it makes a remarkable difference are not thoroughly understood.

*Upscaling the process:* The drive for economy in the semiconductor industry has led to the continuing demand for larger wafers, and hence to larger single crystals both in terms of diameter and length. This leads to bigger melts and growth systems, adding to the inherent complexity of these processes. Some problems – like dislocations in Cz growth of Si – presumed solved as of now, may reappear with upscaling. Also control and reproducibility of the process become even more uncertain with upscaling.

Having discussed issues involving single crystal growth, we shall in the next two sections discuss the theoretical models that account for the major physical phenomena. A brief discussion of the numerical technique developed by our group to solve these equations will also be given. A few sample calculations will then be presented to illustrate the range and utility of these modelling efforts.

#### 4. Theoretical models for transport phenomena and phase change

Crystal growth is a physically rich and mathematically complicated process. The quality of crystals grown depends on many macroscopic and microscopic physical effects. Incorporation of all these effects into the process model is a daunting task. One therefore needs to use discretion and consider the primary effects first, and then examine the effect of secondary parameters. Here theoretical models for all the major phenomena are presented. Less important effects can easily be dropped from the formulation as and when desired.

##### 4.1 Governing equations for flow, heat transfer and species transport

Conservation equations for transport processes in a multiphase system (melt, gas, solid, encapsulant) (in dimensionless form, cylindrical coordinates) (Anselmo *et al* 1993; Zhang & Prasad 1995; Zhang H *et al* 1995; Zou *et al* 1996) can be written as below.

*Continuity:*

$$\frac{\partial}{\partial t}(\bar{\rho}) + \frac{\partial}{\partial x}(\bar{\rho}u) + \frac{1}{r} \frac{\partial}{\partial r}(r\bar{\rho}v) + \frac{1}{r} \frac{\partial}{\partial \theta}(\bar{\rho}w) = 0. \quad (1)$$

*Conservation of momentum:*

$$\begin{aligned} & \frac{\partial}{\partial t}(\bar{\rho}u) + \frac{\partial}{\partial x}(\bar{\rho}uu) + \frac{1}{r} \frac{\partial}{\partial r}(r\bar{\rho}vu) + \frac{1}{r} \frac{\partial}{\partial \theta}(\bar{\rho}wu) \\ &= \frac{\partial}{\partial x} \left( \bar{\mu}_{eff} \frac{\partial u}{\partial x} \right) + \frac{1}{r} \frac{\partial}{\partial r} \left( r\bar{\mu}_{eff} \frac{\partial u}{\partial r} \right) + \frac{1}{r^2} \frac{\partial}{\partial \theta} \left( \bar{\mu}_{eff} \frac{\partial u}{\partial \theta} \right) \\ & - \frac{\partial p}{\partial x} + Gr\beta\theta + S_{inb} + S_{mag} \end{aligned} \quad (2)$$

$$\begin{aligned} & \frac{\partial}{\partial t}(\bar{\rho}v) + \frac{\partial}{\partial x}(\bar{\rho}uv) + \frac{1}{r} \frac{\partial}{\partial r}(r\bar{\rho}vv) + \frac{1}{r} \frac{\partial}{\partial \theta}(\bar{\rho}wv) \\ &= \frac{\partial}{\partial x} \left( \bar{\mu}_{eff} \frac{\partial v}{\partial x} \right) + \frac{1}{r} \frac{\partial}{\partial r} \left( r\bar{\mu}_{eff} \frac{\partial v}{\partial r} \right) + \frac{1}{r^2} \frac{\partial}{\partial \theta} \left( \bar{\mu}_{eff} \frac{\partial v}{\partial \theta} \right) \\ & - \frac{\partial p}{\partial r} - \frac{v}{r^2} + \frac{w^2}{r} - \frac{2}{r^2} \frac{\partial w}{\partial \theta} + S_{inb} + S_{mag} \end{aligned} \quad (3)$$

$$\begin{aligned}
\frac{\partial}{\partial t}(\bar{\rho}\Omega) + \frac{\partial}{\partial x}(\bar{\rho}u\Omega) + \frac{1}{r}\frac{\partial}{\partial r}(r\bar{\rho}v\Omega) + \frac{1}{r}\frac{\partial}{\partial\theta}(\bar{\rho}w\Omega) \\
= \frac{\partial}{\partial x}\left(\bar{\mu}_{\text{eff}}\frac{\partial\Omega}{\partial x}\right) + \frac{1}{r}\frac{\partial}{\partial r}\left(r\bar{\mu}_{\text{eff}}\frac{\partial\Omega}{\partial r}\right) + \frac{1}{r^2}\frac{\partial}{\partial\theta}\left(\bar{\mu}_{\text{eff}}\frac{\partial\Omega}{\partial\theta}\right) \\
- \frac{2\partial\Omega}{r\partial r} + \frac{\partial p}{\partial\theta} + \frac{2\partial v}{r\partial\theta} + S_{\text{turb}} + S_{\text{mag}}.
\end{aligned} \quad (4)$$

Conservation of energy:

$$\begin{aligned}
\frac{\partial}{\partial t}(\bar{\rho}\tilde{C}_p\Theta) + \frac{\partial}{\partial x}(\bar{\rho}\tilde{C}_p u\Theta) + \frac{1}{r}\frac{\partial}{\partial r}(r\bar{\rho}\tilde{C}_p v\Theta) + \frac{1}{r}\frac{\partial}{\partial\theta}(\bar{\rho}\tilde{C}_p w\Theta) \\
= \frac{\partial}{\partial x}\left(\frac{\bar{k}_{\text{eff}}}{\text{Pr}}\frac{\partial\Theta}{\partial x}\right) + \frac{1}{r}\frac{\partial}{\partial r}\left(r\frac{\bar{k}_{\text{eff}}}{\text{Pr}}\frac{\partial\Theta}{\partial r}\right) \\
+ \frac{1}{r^2}\frac{\partial}{\partial\theta}\left(\frac{\bar{k}_{\text{eff}}}{\text{Pr}}\frac{\partial\Theta}{\partial\theta}\right) - \nabla\cdot\mathbf{q}''.
\end{aligned} \quad (5)$$

Conservation of concentration (dopants and impurities):

$$\begin{aligned}
\frac{\partial}{\partial t}(\bar{\rho}C_i) + \frac{\partial}{\partial x}(\bar{\rho}u C_i) + \frac{1}{r}\frac{\partial}{\partial r}(r\bar{\rho}v C_i) + \frac{1}{r}\frac{\partial}{\partial\theta}(\bar{\rho}w C_i) \\
= \frac{\partial}{\partial x}\left(\frac{\bar{D}_{\text{eff}}}{\text{Sc}}\frac{\partial C_i}{\partial x}\right) + \frac{1}{r}\frac{\partial}{\partial r}\left(r\frac{\bar{D}_{\text{eff}}}{\text{Sc}}\frac{\partial C_i}{\partial r}\right) \\
+ \frac{1}{r^2}\frac{\partial}{\partial\theta}\left(\frac{\bar{D}_{\text{eff}}}{\text{Sc}}\frac{\partial C_i}{\partial\theta}\right) \text{ for each species,}
\end{aligned} \quad (6)$$

where  $u$ ,  $v$  and  $w$  are the non-dimensional velocities in  $x$ ,  $r$ , and  $\theta$  directions respectively,  $p$  is the pressure,  $\bar{\rho}$  is the density,  $\Omega (= rv)$  is the swirl velocity in the  $\theta$  direction for rotating systems,  $\Theta$  and  $C$  are the non-dimensional temperature and concentration,  $\bar{\mu}_{\text{eff}}$  is the effective non-dimensional viscosity,  $\bar{D}_{\text{eff}}$  is the effective non-dimensional diffusivity of the species,  $\bar{k}_{\text{eff}}$  is the effective non-dimensional conductivity, and  $\tilde{C}_p$  is the non-dimensional specific heat capacity. The quantities with overbars represent non-dimensional properties, and Gr, Pr and Sc are Grashof, Prandtl, and Schmidt number respectively. The terms  $S_{\text{turb}}$  and  $S_{\text{mag}}$  refer to the source terms for turbulence and magnetic forces,  $S_{\text{mag}} = Ha^2(\mathbf{j} \times \mathbf{B})$ . However, the expression for  $S_{\text{turb}}$  depends on the turbulence model that is employed (Kobayashi *et al.* 1991). Several different models have been used in the simulation of crystal growth (Zhang T *et al.* 1996, 1999).

The following scales have been used to non-dimensionalize the governing equations (1)–(6); length:  $b$  – the crucible radius, velocity:  $v_0/b$ , pressure:  $\rho_o v_o^2/b^2$ , time:  $b^2/v_o$ , density:  $\rho_o$ , dynamic viscosity:  $\mu_o$ , conductivity:  $k_o$ , specific heat:  $C_{p,o}$ , temperature:  $\Theta = (T - T_\infty)/(T_h - T_\infty)$ , and concentration:  $C = C_i/C_{i,o}$ ; where subscript 'o' refers to the phase properties at a reference temperature,  $T_\infty$ ;  $T_h$  – highest temperature in the system;  $v_0$  – kinematic viscosity. In (5),  $\mathbf{q}''$  represents the heat flux, and can be used to account for the term that couples radiation equations with convection–diffusion equations (1)–(5) which can be used for the entire multiphase, multi-component domain. Most of the surface-to-surface thermal radiation modeling of the Cz process considers the optical properties of the crystal to be invariant or non-spectral. However, for several types of crystals, there exist spectral bands, where the crystal can be approximated as either opaque or transparent. A

volumetric radiation model needs to be developed in order to analyse the effect of the encapsulant  $B_2O_3$  layer, high pressure inert gas, and optical behaviour of the crystal materials.

The transport of dopant(s) and impurities can be calculated using (6). There will be  $(n-1)$  equations for the  $n$  species considered; basically one equation for each dopant/impurity.

#### 4.2 Turbulence modelling

The standard  $k-\varepsilon$  model is presented here. The transport equations for kinetic energy,  $k$ , and dissipation,  $\varepsilon$ , can be written as

$$\frac{\partial}{\partial t}(\rho k) + \frac{\partial}{\partial x_i}(\rho u_i k) = \frac{\partial}{\partial x_i} \left( \mu + \frac{\mu_t}{\sigma_k} \right) \frac{\partial k}{\partial x_i} + P_k - \rho \varepsilon \quad (7)$$

$$\frac{\partial}{\partial t}(\rho \varepsilon) + \frac{\partial}{\partial x_i}(\rho u_i \varepsilon) = \frac{\partial}{\partial x_i} \left( \mu + \frac{\mu_t}{\sigma_\varepsilon} \right) \frac{\partial \varepsilon}{\partial x_i} + \frac{\varepsilon}{k} [C_{1\varepsilon} P_k - C_{2\varepsilon} \rho \varepsilon] \quad (8)$$

where  $\mu_t = C_\mu k^2/\varepsilon$ , is the turbulence viscosity and  $P_k$  is the turbulence production term.

The renormalization group (RNG)  $k-\varepsilon$  model also belongs to the  $k-\varepsilon$  family of models. The model equations in their RNG form are similar to the above equations (Yakhot & Orszag 1986). However, the effect of the swirl on turbulence is included in the RNG model, which enhances the accuracy for swirling flows, and the RNG theory also provides an analytically derived differential formula for effective viscosity that accounts for low-Reynolds-number effect. The RNG  $k-\varepsilon$  formulation is considered to be a better model for the flow field simulation of the Cz-type process. The wall function approach has been used in the near wall region (Patel *et al* 1985) because of the limitation on the number of nodes that can be employed in complex materials processing problems. For example, a large number of insulating components and baffles exist in a Czochralski (Cz) growth furnace, that makes it very difficult to use very fine grids in every wall region. The formulation for wall functions in a non-orthogonal coordinate system can be found in Thakur *et al* (1996). Details of the implementation of different turbulence models for the simulation of Cz and LEC growth can be found in Zhang T *et al* (1996).

#### 4.3 Interface and boundary conditions

Czochralski growth is characterized by the presence of interfaces between two different fluids – melt/gas interface in low pressure Cz growth, and melt/encapsulant, encapsulant/gas interfaces in high pressure Cz growth. Treatment of these fluid/fluid interfaces is rather complicated, since the position of the interface is not known *a priori*.

High pressure Cz growth is characterized by the presence of encapsulant/melt interface and a melt/gas interface. We characterize the height of the melt/encapsulant interface above the crucible bottom as  $H_1(r, t)$ , and that of the encapsulant/gas interface as  $H_2(r, t)$  as shown in figure 7. Since the viscosity of the boric oxide encapsulant is very high, this interface can be taken as flat, or  $H_2(r, t)$  is independent of  $r$  (figure 7). At the encapsulant/gas interface, no-slip conditions can be applied for the hydrodynamic boundary conditions. Hydrodynamic boundary conditions at the encapsulant/melt interface are treated on the basis of three principles (Batchelor 1967): (1) fluid particles at the interface must remain attached to the interface (kinematic condition), (2) difference in tangential

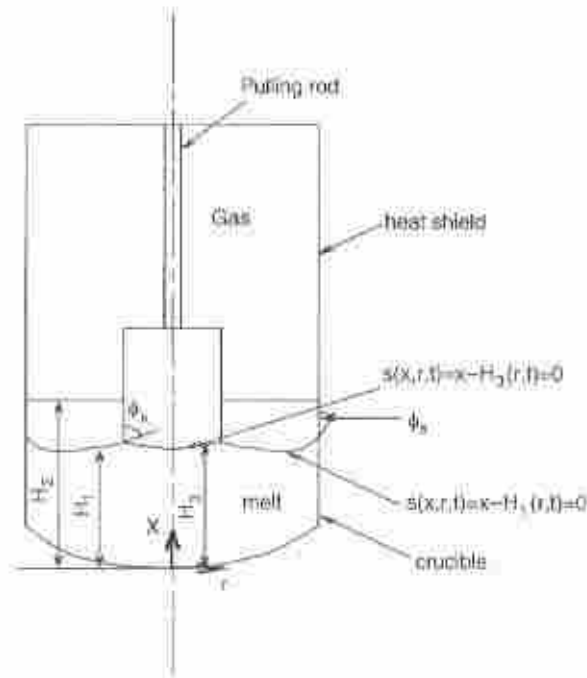


Figure 7. Schematic illustrating the various free surfaces and the solidification interface in LEC growth.

force components due to stress on both sides of the interface must be balanced by the forces due to surface tension gradients, and (3) difference in normal force components on both sides of the interface, due to the stress components, must be balanced by the normal surface tension force due to the curvature of the interface. These three conditions translate to the following.

Conditions at melt/encapsulant interface:

$$u = \frac{\partial H_1}{\partial t} + v \frac{\partial H_1}{\partial r}, \quad (7)$$

$$\frac{\partial v}{\partial n} - \frac{\partial u}{\partial r} = \frac{Ma \partial \theta}{Pr \partial n}, \quad (8)$$

$$\frac{\partial^2 H_1 / \partial r^2}{\left[1 + (\partial H_1 / \partial r)^2\right]^{3/2}} + \frac{\partial H_1 / \partial r}{r \left[1 + (\partial H_1 / \partial r)^2\right]^{1/2}} = Bo(H_1 - \Delta p \cdot Fr + 2\partial u / \partial n \cdot Fr), \quad (9)$$

where  $Ma$  is the Marangoni number,  $Bo$  is the Bond number, and  $Fr$  is the Froude number.

Since (9) contains second-order spatial derivatives in  $H_1$ , two boundary conditions are needed to solve for  $H_1(r, t)$ . These are given by the unique contact angles the melt/encapsulant interface makes with the crystal, and the crucible;  $\phi_A$ ,  $\phi_B$ ;  $n$  and  $\tau$  are the coordinates along the normal and tangential directions to the surface (figure 7); and  $\theta$  refers

to the non-dimensional temperature. These conditions can be expressed as

$$\frac{\partial H_{1,c}}{\partial r} = \tan(\phi_s - 90^\circ) \quad \text{and} \quad \frac{\partial H_{1,c}}{\partial r} = \tan(\phi_k - 90^\circ). \quad (10)$$

The concept of a fixed wetting angle was adapted by Bardsley *et al.* (1974) for the meniscus defined crystal growth. Surek & Chalmers (1975) conducted experiments, which verify that the angles,  $\phi_s$ ,  $\phi_k$ , are well defined for a particular material, for growth in a particular orientation. These angles are apparently independent of the growth rate. These conditions, along with the known volume of the melt, provide the hydrodynamic boundary conditions at the melt/encapsulant interface, as well as uniquely fix its shape –  $H_1(r, t)$ . The constant height of the encapsulant/gas interface  $H_2(t)$  is determined by applying the constancy of volume of the encapsulant,

$$\int_{R_c}^1 (H_2 - H_1) r \, dr = \text{const.} \quad (11)$$

Thermal boundary conditions at these interfaces are based on simple temperature continuity, and energy balance and will not be discussed further. More elaborate details of the treatment are presented by Zhang H *et al.* (1998).

The low pressure Czochralski growth system is characterized by a melt/gas interface: the treatment of which follows from the same principles elaborated above.

*Conditions at the crystal/melt interface:* The solidification of a pure substance is modelled with a fixed fusion temperature  $T_f$ , implying the presence of a sharp well-defined interface, defined by

$$s(x, r, t) = H_3(r, t) - x = 0.$$

For hydrodynamic boundary conditions, the interface can be treated as a solid/fluid interface, with no-slip conditions. The temperature boundary condition is simple, since the temperature of the interface is at the fusion temperature,  $T_f$ . The position of the interface and its motion is defined by the energy balance across it as follows,

$$\rho_s h_{sl} (U_{m,n} - U_s(t) \mathbf{e}_x \cdot \mathbf{n}) = k_s \frac{\partial T_s}{\partial n} = k_l \frac{\partial T_l}{\partial n} \quad (12)$$

where the densities of the crystal and melt phases are assumed to be equal,  $h_{sl}$  is the specific heat of fusion, subscripts  $s$  and  $l$  denote solid and liquid respectively,  $\mathbf{n}$  is the normal vector from solid to melt,  $\mathbf{e}_x$  is the unit vector in the  $x$  direction, and  $n$  is the coordinate in the normal direction. In (12),  $U_{m,n} = (\partial H_3 / \partial t) \mathbf{e}_x$  is the velocity of the crystal-melt interface, and  $U_s(t)$  is the pull velocity. An expression for the movement of the crystal-melt interface can be obtained as follows,

$$\frac{\partial H_3}{\partial t} - U_s(t) = \frac{Ste_s}{Pr_l} \left( \kappa_s \frac{\partial \theta_s}{\partial n} - \kappa_l \frac{\partial \theta_l}{\partial n} \right) \left[ 1 + \left( \frac{\partial H_3}{\partial r} \right)^2 \right], \quad (13)$$

and the pull rate  $U_s(t)$  can be calculated from

$$U_s(t) \equiv -(1 - Rr^2) \left\{ \frac{Ste_s}{Pr_l} \left( \kappa_s \frac{\partial \theta_s}{\partial n} - \kappa_l \frac{\partial \theta_l}{\partial n} \right) \left[ 1 + \left( \frac{\partial H_3}{\partial r} \right)^2 \right] \right\}_{r=R} \quad (14)$$

where  $Rr$  is the radius ratio (crystal-to-crucible radii),  $Ste$  the Stefan number,  $\kappa$  the conductivity, and  $\theta$  the non-dimensional temperature. More details can be found in Kopetsch (1989), and Zhang H *et al* (1998).

The boundary condition for concentration of species at the solid/liquid interface is

$$-(1/Sc)\nabla C \cdot \mathbf{n} = C(1 - k_0)V_p \cdot \mathbf{n}, \quad (15)$$

where  $k_0$  is the distribution coefficient of the dopant.

*Thermal boundary condition at the crucible wall:* Temperature conditions at the crucible wall (figure 6) are most difficult to define. The most popular heating system consists of an inductor (r.f. coil), which is made of a copper coil, through which an alternating current is passed, and a conducting susceptor (generally of graphite), where electric current is induced and generates heat by ohmic dissipation. Recently, resistance heaters have become more popular. Modelling these induction heaters is a difficult task, since it involves the solution of Maxwell's equations. Although it is feasible to model radio-frequency heating, most of the studies assume either a constant temperature or flux at the crucible wall.

#### 4.5 Numerical strategy

The modelling of Cz, LEC, and Bridgman processes is a complicated task due to the coupled nature of heat conduction, convection, thermal radiation, fluid flow, and other transport phenomena. The task of modelling also becomes difficult due to geometric complexities, moving interfaces, high temperatures, and disparate time scales. Special numerical strategies are therefore needed to successfully model the high pressure crystal growth processes. The chief tenets of the strategy adopted by Zhang, Prasad and co-workers, found in Zhang & Prasad (1995), Zhang H *et al* (1995) are as below.

(a) Since crystal growth is a very slow process, the whole growth can be approximated as a series of quasi-steady states, each for a given crystal height and the corresponding melt volume. For a given quasi-steady state, the crystal and melt heights (volumes) are fixed and the method outlined below is adopted to solve for the flow, temperature and concentration fields, and interface/free surface geometry. The crystal and melt heights are then updated for the next quasi-steady state, and the calculations are repeated. Thus, the intractable task of obtaining thermal, flow and other information continuously through the whole growth period has been broken into the more modest task of obtaining such information at discrete intervals.

(b) A special curvilinear multizone adaptive grid generation scheme (MAGG) for generation, redistribution and clustering of grids is implemented. Based on constrained adaptive optimization of the grid characteristics, smoothness, orthogonality, concentration, and grid inertia integrals (Zhang & Moallemi 1995), this scheme is able to preserve internal surfaces and make them coincide with some gridlines. It also allows grids to move adaptively as the solution progresses and/or domains change. The generated grids are always smooth and orthogonal, maintain slope continuity, and cluster in the regions of interfaces/free surfaces and large gradients. The curvilinear feature ensures accurate representation of the geometry.

(c) A non-orthogonal curvilinear finite volume technique is used to discretize the various transport equations. A non-staggered grid formulation is employed and is given by

Zhang H *et al* (1996). Consequently, the algorithm for fluid flow calculations is based on the solutions of a pressure equation to obtain the pressure field and a pressure-correction equation to correct the predicted velocities. The momentum interpolation scheme is employed in the discretization of pressure and pressure correction equations:

(d) The procedure employed is shown in figure 8. Once the melt and crystal heights are fixed, initial grids are generated, and the finite volume solver is employed to predict the velocity, temperature and concentration fields. The temperature distribution obtained from the finite volume solver serves as input to the radiation module. The resultant heat flux is then fed back to the finite volume solver and the temperature, velocity and concentration fields are calculated again. This procedure is repeated till converged fields have been obtained. The solidification interface and free surfaces are then updated based on energy balance and stress balance respectively. The grids are then made to adapt to the new position of the interfaces, and the field variable calculations are performed all over again. This iteration is repeated until the interfaces stop moving. At this point the thermal and other fields and the interface shapes for the quasi-steady state represented by a given crystal height and melt height are known. The temperature field is then passed to a stress module for stress calculations. The geometry is then adjusted for the next quasi-steady step – melt height and crystal height are changed – and the process is repeated.

## 5. Modelling of defects in as-grown crystals

Single crystals grown from the melt are seldom perfect. They contain many defects – point defects, precipitates, dislocations, agglomerations of point defects etc. Here we shall basically treat dislocations, which are the main defects in III–V and II–VI compounds.

### 5.1 Dislocations

One of the major types of defects in semiconductor materials like Si, Ge, InP, GaAs are line defects or dislocations. These dislocations are present in as-grown bulk material because of a variety of reasons such as thermal stresses, excess point defects precipitating to form prismatic dislocation loops etc. They can also be introduced into the material while processing (e.g., diffusion and ion implantation), and when bulk materials are used as substrates for epitaxial growth, dislocations in the substrates can propagate into the films.

The presence of dislocations is harmful to device performance; a few deleterious effects are discussed by Jordan *et al* (1986). Though some important questions remain to be answered on the origin of dislocations, there is general consensus on some of the main phenomena which might be responsible for them.

(a) The condensation of excess point defects present during growth, at high temperatures, as prismatic, or  $1/3$  {111} Frank dislocation loops. This mode is important when there are inclusions, and is also closely related to the effect of non-stoichiometry.

(b) The use of a defective seed, containing in-grown dislocations. This can result in dislocations gliding from the seed to the growing crystal, where they are multiplied under thermal stresses. Dash (1958) pioneered the necking technique, which will be discussed later, to prevent this phenomenon.

(c) A systematic study has shown the role that melt stoichiometry plays in the generation of dislocations. Brice & King (1966) have reported on the influence of melt stoichiometry on the dislocation density in LEC-grown GaAs. They have shown that the partial pressure of As during the growth of GaAs is an important parameter to control the dislocation

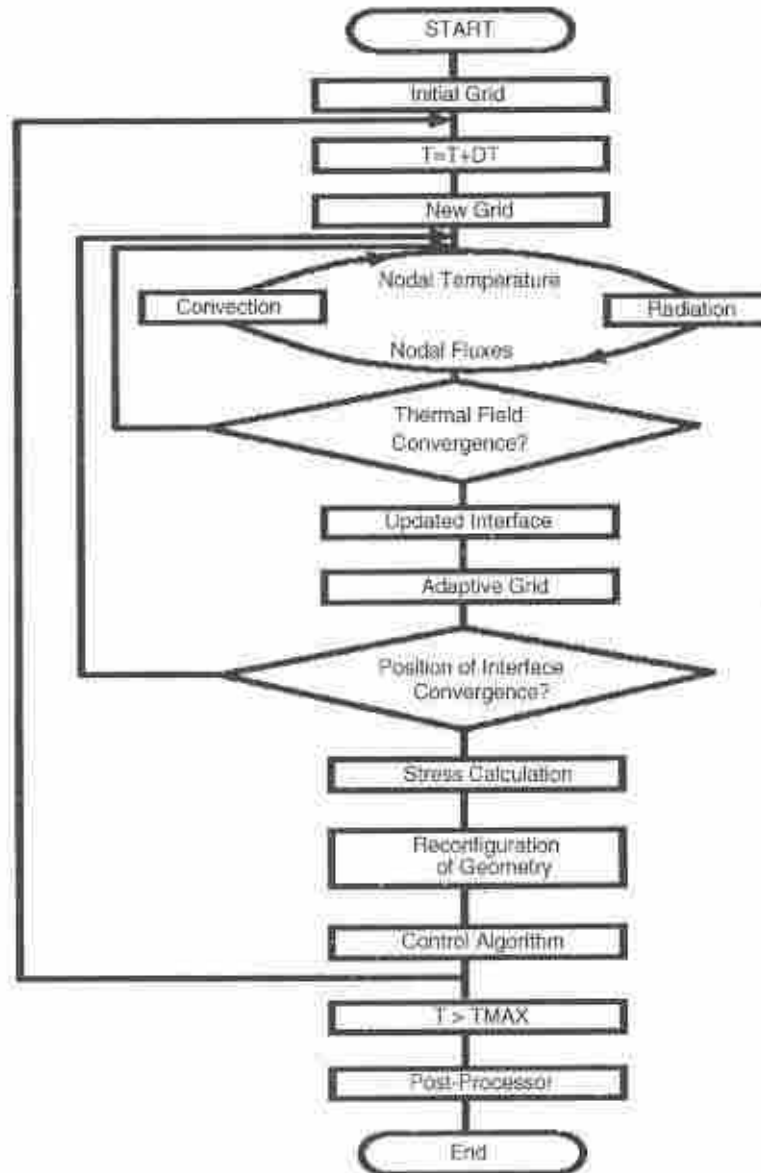


Figure 8. Flowchart elaborating the algorithm of solution of the transport equations along with stress calculations of the crystal growth process.

density in horizontal Bridgman-grown crystals. Their observation was confirmed by Parsey *et al.* (1982), who grew small GaAs crystals using the horizontal Bridgman method, and controlled the As vapour pressure by controlling the As source temperature. They found that crystals of minimum dislocation density could be obtained for an arsenic temperature of 617°C, which corresponded to a stoichiometric melt composition. Any deviation from the temperature or stoichiometry gave high dislocation densities, the dislocations generated

by these phenomena are essentially due to the condensation of point defects, forming dislocation loops.

(d) Another cause of nucleation of dislocations may be poor epitaxy during growth (Dashi 1958). Dislocations can form at the seed or in other parts of the crystal during growth without multiplication of those already present. This occurs when the liquid comes into contact with solid, which is either contaminated or is at too low a temperature to enable perfect epitaxy. The contamination may be impurities – specks of solid matter – floating in the melt, formation of oxide on the surface of the hot crystal etc.

(e) Surface damage of the growing crystal can also act as a seed for nucleation of dislocations. This effect is expected to be negligible in the Czochralski system, since there is no chance of surface damage here.

(f) Inhomogeneities in dopant distribution result in striations in the growing crystal. These result from instabilities at the growth interface, caused by adjacent layers of different dopant concentration, along the growth direction. The fluctuations in composition of the different layers may be up to the order of 10%. Due to the different thermal expansion of these adjacent layers, the thermal stresses in the material may get exacerbated, resulting in increasing the dislocation density. Another source can be the lattice mismatch present between such layers, due to the variation in the lattice parameter – this may give rise to misfit dislocations, which provide the seed dislocations for multiplication under the action of thermal stress (Voekl 1994). This method of nucleation of dislocations may be important in the early stage of solidification, when the temperatures are high.

After the nucleation of the first dislocations in the growing crystal by any of the above mechanisms, they are rapidly multiplied and propagated under the action of thermal stresses. Since crystal growth is inherently a non-equilibrium process, involving heat transfer through the crystal, the presence of temperature gradients in the crystal is mandatory. The crystal acts as a medium through which heat is transferred from the melt to the ambient. The heat enters the crystal at the crystal/melt interface, and leaves through the external surfaces by radiation and convection. Thus the core of the crystal is hotter than the periphery, and the bottom of the growing crystal is hotter than the top. These temperature gradients give rise to differential expansions of different parts of the crystal, and consequently thermal strains and stresses. Perhaps the most conclusive proof of the role of thermal stresses in dislocation generation is the successful attempt to grow dislocation free crystals, by maintaining low thermal gradients in the crystal (Shinoyama *et al* 1980). Attempts to model dislocation generation in literature have centred around two models, the critical resolved shear stress (CRSS) model and the Alexander–Haasen model.

## 5.2 CRSS model

The critical resolved shear stress (CRSS) model was introduced by Jordan *et al* (1980) who recognized that elemental III-V and II-VI semiconductors crystallize in the diamond or the zincblende structure, which has twelve different slip systems. These slip systems corresponds to the three  $\langle 110 \rangle$  directions on each of the four  $\{111\}$  slip planes. In a model, the crystal is assumed to be a thermal elastic medium, and once the temperature field in the crystal has been calculated, these are fed to a finite element code to calculate the thermal elastic stresses. Usually, the elastic crystal is assumed to have cubic symmetry, and the constitutive equations have three parameters, instead of the usual two in the

isotropic case. The calculated stresses are then resolved on to the twelve slip systems, and the resolved shear stresses along these slip systems are calculated.

Jordan *et al* (1980) assumed that the dislocation density is proportional to the glide or plastic strain, which is caused when the resolved shear stress,  $\sigma_{RS}$ , on a slip system exceeds a certain critical value, termed the critical resolved shear stress,  $\sigma_{CRS}$ . The excess shear stress is the driving force for plastic deformation in that slip system, and the plastic strain is assumed proportional to the excess shear stress. The excess shear stress on all the slip systems is then summed up and the resultant sum,  $\sigma_{ex}$ , is used to characterize the dislocation density. Mathematically,

$$\sigma_{ex} = \sum_{i=1}^{12} |(\sigma_i^e)|,$$

where  $\sigma_i^e$  is the excess resolved shear stress and is defined by,

$$\begin{aligned} \sigma_i^e &= |(\sigma_{RS})_i| - \sigma_{CRS}, & \text{for } |(\sigma_{RS})_i| > \sigma_{CRS}, \\ \sigma_i^e &= 0, & \text{for } |(\sigma_{RS})_i| < \sigma_{CRS}. \end{aligned}$$

The resolved shear stress  $\sigma_{RS}$  is calculated by

$$\sigma_{RS} = \sigma_{ij} n_k m_i,$$

where  $\sigma_{ij}$  are the components of the stress tensor,  $n_k$  are the components of the unit vector normal to the slip plane and  $m_i$  are the components of the corresponding slip direction.  $\sigma_{ij}$ ,  $n_k$ ,  $m_i$  are all referred to the crystallographic axis. Generally, the value of the  $\sigma_{CRS}$  depends on the temperature, doping levels etc.

This formalism, though lacking in quantitative results, gives a qualitative description of the dislocation distribution in the grown crystal, which has been shown to be consistent with experimental observations. For example, the model predicts a four-fold symmetry of dislocation distribution on (100) wafers, and a six-fold symmetry on (111) wafers, both observations being consistent with the experimentally obtained etch pit distributions (Jordan *et al* 1986). This theory has been the basis for a number of studies on the effect of various process parameters on dislocation densities, for both the Czochralski and the VGF growth processes. Examples of these have been given by Miyazaki *et al* (1990), Chen & Holmes (1983), Jordan *et al* (1993), Schvezov *et al* (1989) and Chen *et al* (1997). The model, though useful, provides only qualitative information and cannot predict any reliable quantitative details. Moreover, in the case of Czochralski growth, qualitative agreement is good only near the seed of the crystal. On the interface side of the crystal, the agreement is rather poor (Jordan *et al* 1986).

### 5.3 Alexander-Haasen model

The Alexander-Haasen model (Alexander & Haasen 1968) is a more fundamental, micro-dynamical, phenomenological model describing the plastic strain rate on a slip system in terms of dislocation dynamics. It was introduced to explain the stress-strain behaviour of elemental and compound semiconductors like Si, Ge, InSb, during a uniaxial compression or tensile test, conducted at a constant strain rate, on a crystal oriented for single slip. The most common way of obtaining these curves is the compression test. This is done in a

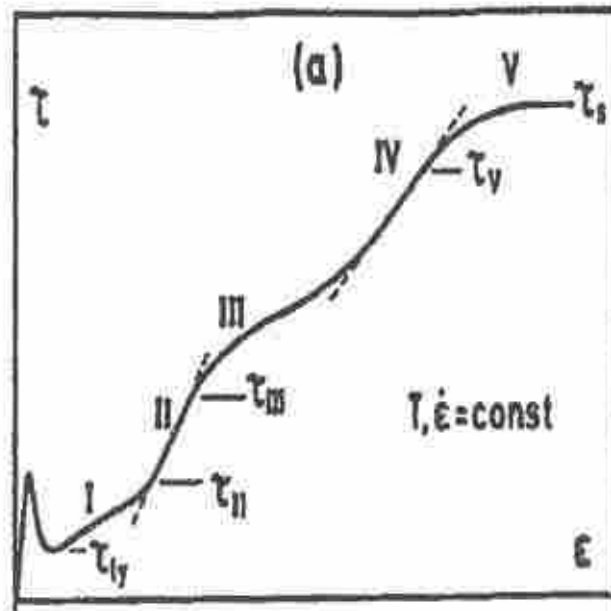
constant displacement-rate machine, in which the specimen is kept between two rigid crossheads, while one of them moves at a fixed speed. The deflection of a stiff ring attached to the crosshead measures the axial force on the specimen at any instant. The force is recorded as a function of the crosshead displacement, which can then be converted into shear stress–shear strain curves from the specimen dimensions. An example of these is figure 1 of Seithof (1992) which shows a series of shear stress–shear strain, obtained at different temperatures, for a crystal oriented in the single slip  $\langle 123 \rangle$  direction.

Figure 9 shows a detailed view of one of those stress–strain curves. At low temperatures, three deformation stages following the upper and lower yield points are observed: a stage of low work hardening (I), a stage of strong work hardening (II), and a stage of increasing softening (III), where recovery processes operate in the crystals exposed to an external stress – dynamical recovery. At high temperatures, two further stages appear: a new hardening stage (IV), and a second recovery stage (V). The most striking aspect of this curve is the presence of an upper and a lower yield point. The Alexander–Haasen model was first put forward to explain this unique yield point behaviour.

The central tenet of the theory is the introduction of a variable  $N$  to denote the dislocation density in the crystal. The plastic shear-strain rate on the only active slip system is given by the Orowan relation,

$$\frac{d\gamma_{pl}}{dt} = bNv, \quad (16)$$

where  $b$  is Burgers vector of dislocation,  $v$  mean velocity of the dislocations, and  $\gamma_{pl}$  plastic shear strain on the only active slip system. Since, there is only one active slip plane in the



**Figure 9.** Generic shape of the shear stress versus shear strain on the main slip system, for single crystals of elemental and compound III–V semiconductors deformed at constant strain rate in single slip.

crystal, the axial component of the macroscopic plastic strain tensor,  $\varepsilon_{pl}$ , is given by

$$\dot{\varepsilon}_{pl} = \dot{\gamma} \tau_{pl}$$

The velocity of dislocations in the slip system,  $v$ , is dependent on the resolved shear stress of that system, and has been found experimentally (Chaudari *et al* 1962), to be of the form:

$$v = v_0 (\tau_{eff}/\tau_0)^m \exp(-Q/k_B T), \quad (17)$$

where  $m$ ,  $\tau$ ,  $Q$ , and  $k_B$  are empirical constants depending on the semiconductor material and its doping. The effective resolved shear stress on a dislocation is given by,

$$\tau_{eff} = \tau - A\sqrt{N}, \quad (18)$$

where  $\tau$  is the externally applied shear stress on the active slip system, and  $A\sqrt{N}$  is the backstress on a given dislocation due to the neighbouring ones, which resist its movement through interaction. The form square root dependence of the back-stress on  $N$  is a classical one and was first derived by Taylor (1934) based on an arrangement of parallel dislocations on a slip plane. Though the actual arrangement of the dislocations – the microstructure – was found to be much more complicated than was assumed by Taylor, this form of the back-stress has been found to be valid under a wide range of conditions and is widely used in work-hardening theory (Nabarro *et al* 1964). The dislocations multiply as they move resulting in evolution of the dislocation density. It is assumed that each moving dislocation leaves behind  $\delta$  loops on travelling unit distance. Thus the evolution of dislocation density can be modelled by,

$$(dN/dt) = \delta Nv. \quad (19)$$

On experimental evidence,  $\delta$  is assumed to be directly proportional to the effective stress  $\tau_{eff}$ . Therefore,  $\delta = k\tau_{eff}$ . Combining (16), (17), (18), and (19), we obtain a set of two equations

$$\frac{d\varepsilon_{pl}}{dt} = \phi b N v_0 \left( \frac{\tau - A\sqrt{N}}{\tau_0} \right)^m \exp\left(-\frac{Q}{k_B T}\right), \quad (20)$$

$$\frac{dN}{dt} = k N v_0 \left( \frac{\tau - A\sqrt{N}}{\tau_0} \right)^{m+1} \exp\left(-\frac{Q}{k_B T}\right). \quad (21)$$

Equations (20) and (21) form a complete set of phenomenological models, which given the externally applied shear stress  $\tau$ , can model the evolution of the plastic strain and dislocation density with time. They describe the yield region in the curve shown in figure 10 rather well, and can account for the occurrence of the upper and lower yield stress. In the stress-strain curve shown in figure 10, the total strain rate, which is the sum of elastic and plastic strain rates is maintained constant,

$$\dot{\varepsilon}_{tot} = \phi(\dot{\tau}/G) + \dot{\varepsilon}_{pl} \quad \text{or} \quad \dot{\varepsilon}_{tot} = \phi(\dot{\tau}/G) + \phi b N v. \quad (22)$$

In semiconductor crystals of high structural perfection, the built-in dislocation density is low, hence a constant total strain rate can initially be maintained only if the elastic

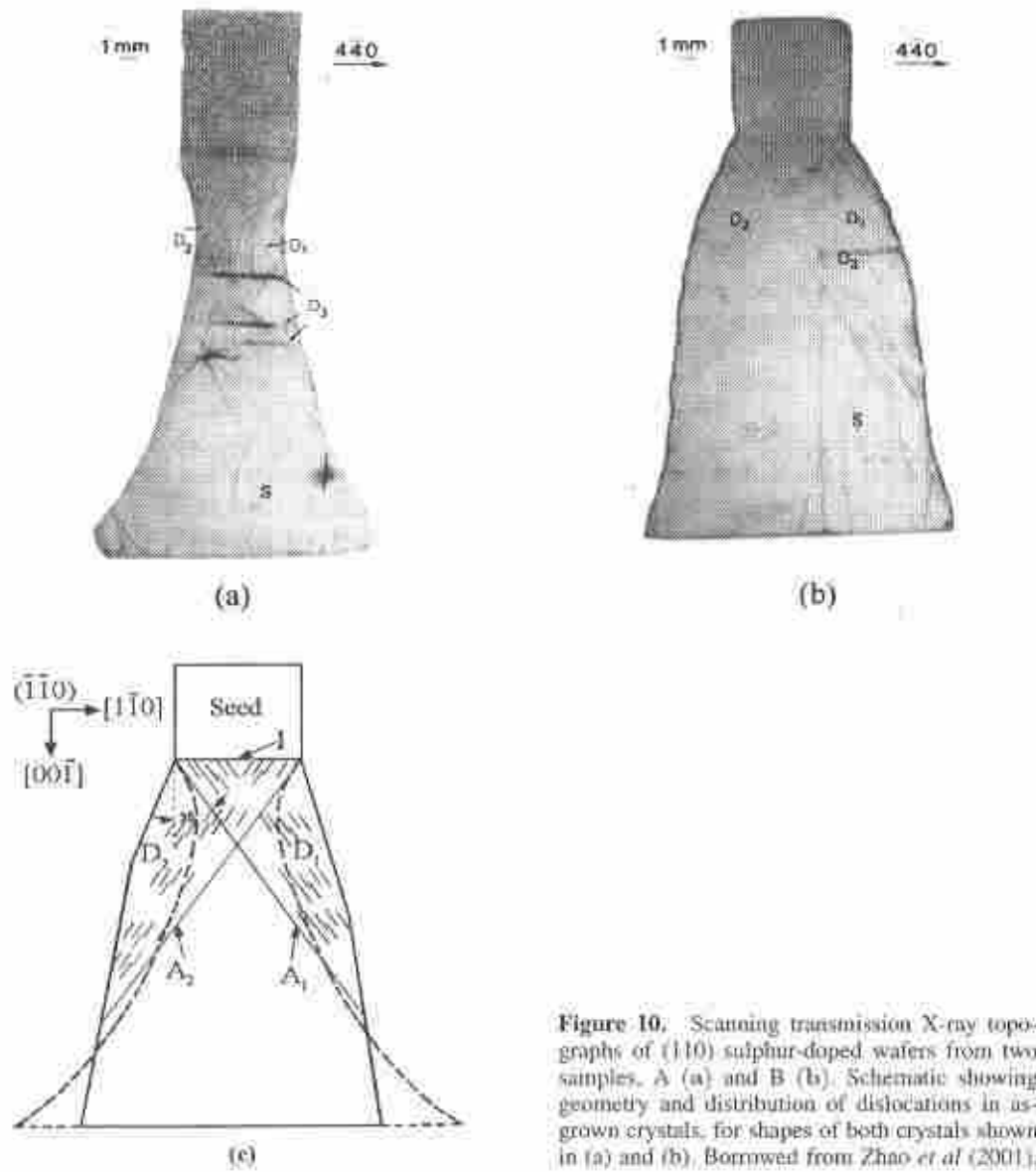


**Figure 10.** Scanning transmission X-ray topographs of (110) sulphur-doped wafers from two samples, A (a) and B (b). Schematic showing geometry and distribution of dislocations in as-grown crystals, for shapes of both crystals shown in (a) and (b). Borrowed from Zhao *et al.* (2001).

deformation rate  $\dot{\gamma}/G$  produces a high stress. Then according to (17), the high effective stress thus produced gives the existing dislocations a high velocity. The few existing dislocations then multiply, increasing the dislocation density  $N$ ; the velocity can then decrease according to the prescribed strain rate, as per (22). This, in turn, decreases the stress continuously until dislocation multiplication leads to dislocation interaction, i.e., work-hardening represented by  $A\sqrt{N}$ . Finally, the applied stress must again rise to keep the effective stress, i.e., the dislocation velocity up to the level demanded by the constant imposed total strain rate  $\dot{\epsilon}_{tot}$ . The foregoing arguments thus explain the occurrence of an upper ( $\tau_{u\dot{\gamma}}$ ) and a lower yield stress ( $\tau_{l\dot{\gamma}}$ ). The empirical constants in the above model are obtained by fitting the equations to experimental data.

Excellent reviews of this model have been presented recently by George & Rabier (1987), and Rabier & George (1987). Sumino & Yonenaga (1993) have noted some peculiarities of the model – sharpness of the yield points etc. – and have suggested modifications. Alexander (1986) has given an excellent and comprehensive review of the deformation of elemental semiconductors, Si and Ge. Siethoff and coworkers (see the review by Siethoff 1992) have conducted many significant studies in this field over a span of three decades, investigating the various stages of the deformation behaviour of semiconductors.

Voekl *et al* (1987) first used the above model to study the dislocation generation in the Cz system. In their analysis, the entire thermal and thermal-elastic stress history of a given particle in the crystal, from the particle evolution at the melt/crystal interface to the end of the growth process, is determined. The thermal-elastic stress history, so determined, is used to determine the resolved shear stress history on the highest stressed slip system; an unstated assumption by Voekl *et al* (1987) is that the same slip system is most stressed throughout the growth history of the particle. The resolved shear stress history is designated  $\tau_i^{el}(t)$ . Voekl assumes that as the plastic deformation proceeds, the resolved shear stress relaxes or is dissipated by plastic strain, and the residual elastic stress  $\tau_{er}(t)$  is the driving force behind the plastic deformation, i.e.,  $\tau_{er}(t)$  takes the place of  $\tau$  in (20) and (21). The relaxation process is then described by,

$$\frac{d\tau_{er}(t)}{dt} + \frac{G d\varepsilon_{pl}}{\phi \cdot dt} = \frac{d\tau_i^{el}(t)}{dt}. \quad (23)$$

In conjunction with (23), (20) and (21) are used with  $\tau$  replaced by  $\tau_{er}(t)$ .

$$\frac{d\varepsilon_{pl}}{dt} = \phi b N v_0 \left( \frac{\tau_{er}(t) - A\sqrt{N}}{\tau_0} \right)^{m_0} \exp\left(-\frac{Q}{k_B T}\right), \quad (24)$$

$$\frac{dN}{dt} = k N v_0 \left( \frac{\tau_{er}(t) - A\sqrt{N}}{\tau_0} \right)^{m_0+1} \exp\left(-\frac{Q}{k_B T}\right). \quad (25)$$

Since, the thermal-elastic history  $\tau_i^{el}(t)$  has already been determined from the thermal history of the crystal, through a finite element code, (23), (24), (25) are integrated simultaneously to obtain the final dislocation density  $N$ . The dislocation density, in the volume element, after it just emerges out from the melt is taken as a fixed constant,  $N_0$ . This is just a boundary condition

$$N|_{t=0} = N_0.$$

However, Voekl *et al* (1987) claim that the final values of  $N$  are reasonably independent of the chosen value of  $N_0$ . It is apparent that a choice of  $N_0 = 0$  will lead to a singularity.

Voekl justifies his assumption of single slip with an argument that 'an exponential dependence of plastic deformation from stress will cause the highest loaded slip system to act and thus release the stresses on all other slip systems. Maroudas & Brown (1991) introduced an isotropic generalization of the plastic strain response in the A-H model and performed what they called an integrated analysis of crystal growth. Their analysis is dictated by the need for fast computer modelling of the growth process, and is achieved through an asymptotic analysis. Tsai (1991) has generalized the Alexander-Haasen model to an isotropic plastic response, instead of assuming deformation on the highest stresses

slip system, and applied it to the bulk crystal growth. Tsai *et al.* (1993) later formulated a multislip generalization of the A-H model, involving all the twelve slip systems that are active in semiconductor crystals. Lambropoulos & Wu (1996) recently applied the model to LEC growth of GaAs, and investigated the effect of the shape of the interface on final dislocation generation. Miyazaki recently implemented this model in the simulation of bulk Cz growth using a finite element technique (Miyazaki & Okuyama 1998; Miyazaki & Kuroda 1998; Miyazaki & Kuroda 1999).

The driving force behind deformation in the growing crystal is the thermal strain. Since the thermal strains are small, the deformations are likely to fall within the yield region in figure 9, thus justifying the use of the A-H model. However, there is no evidence that the thermal loading would favour the single slip scenario – thus single slip models are on somewhat slippery ground. Moreover, as noted earlier, stages IV and V in figure 9 appear only at high temperatures. Higher temperatures are characterized by a shrinkage of the stress-strain curves – the various stages occur at lower strains. This indicates that phenomena like cross-slip, and climb of dislocations, which dominate the later stages, become important at lower strains for deformation at high temperatures. Thus, at temperatures approaching the melting point of the crystal – for which few data are available – these phenomena might be important even in the yield-point region. Thus a multislip generalization of the A-H model is needed, with provisions for high temperature phenomena like cross-slip, climb, dislocation annihilation etc. A recent model (Moosbrugger & Levy 1995; Moosbrugger 1995) considers several of these features for CdTe crystals, and is the most advanced of the A-H variants.

However, it should be noted that the solution of a visco-plastic boundary value problem using these complicated models is a very expensive process requiring the use of efficient computational techniques and powerful machines. A judicious choice of model, based on a cost benefit analysis of the improvement in result-versus-effort, ought to be made. For simple qualitative guidelines, the Jordan model is the simplest and most useful, both in terms of the formulation and effort needed to use it. However, it should be kept in mind that many aspects of dislocations are still unresolved. At the beginning of the section, several mechanisms have been cited as probable mechanisms of the introduction of dislocations in the growing crystal. None of these have been investigated in any detail. The theories detailed above concentrate only on the propagation of the existing dislocations under the influence of thermal stresses.

## 6. Numerical simulation

As delineated above, the issues in single crystal growth are many, and efforts have made in recent times to put them in perspective and bring together the physics of various processes and their interrelationships in a massive numerical model. While the development of powerful computers and advanced numerical algorithms can make these calculations feasible to a great extent, roadblocks exist in the form of limited understanding of the physics of certain phenomena, the lack of suitable models to describe them, and the diverse time scales needed to solve such problems. While the ultimate goal of these modelling efforts would be to model the entire growth process from beginning to end, establish a precise connection between the macroscopic parameters and crystal quality, set up elaborate growing programs for crystal growers, help in formulating control schemes, and finally help in designing more sophisticated control systems, current modelling efforts are still down to earth. They aim more at supplementing theoretical studies, providing practical

guidelines to crystal growers, and helping in the design of the upscaled system. A recent example of such a simulation will now be presented.

It is well-known that a dislocation-free Si single crystal can be grown employing a high pull rate and a technique termed necking (Dish 1958). The term "necking" arises from the shape of the crystal being grown. The diameter of the growing crystal is decreased from the seed to a minimum, before it is increased again. Thus the crystal has a neck of minimum diameter. Recently, attempts have been made to extend the necking technique to sulphur-doped LEC-grown InP (Zhao *et al* 2001). The InP crystals so grown were analysed using synchrotron white beam X-ray topography (SWBXT).

Figures 10a & b, present the scanned transmission topographs of the crystals grown, recorded from two (110) InP wafers, samples A and B respectively. Figure 10c shows a geometric sketch of the dislocations in both the crystals. An analysis of these topographs reveals that most of the dislocations in LEC-grown InP crystals originate from the seed-crystal interface, propagate via slip planes, and eventually exit the crystal through the periphery of the necked region. Based on this mechanism, dislocations exist only in the outer regions (dislocation regions) of the grown crystal separated by the four {111} planes which are extended from the four edges of the seed bottom. In the cross-sectional view of figure 10c, two of these planes, (111) and ( $\bar{1}\bar{1}\bar{1}$ ) are represented by lines  $A_1$  and  $A_2$  respectively. It is apparent that we can effectively limit the dislocation region by choosing the proper growth conditions, i.e., by adopting the necking technique. As shown in figure 10c, the narrow necked portion of sample A makes the dislocation region much smaller than that of sample B. It means that the dislocations emerging from the seed-crystal interface in sample A slipped out of the neck in much shorter distances than that in sample B. A pyramid-shaped crystal, which is nearly dislocation-free was quickly formed below the dislocation regions. This dislocation free region prevailed until the crystal diameter reached 15 mm, when the dislocations reappeared. Growth near the 15 mm diameter region was also associated with the problems of intense twinning and large dislocation densities. Consequently this portion of the grown crystal is not shown in figures 10a–c. The existence of this critical diameter of around 15 mm was also reported by other authors (Shinoyama *et al* 1980), but the reason for this was never made clear.

To supplement the study detailed above, a numerical study was carried out with the help of the MASTRAPP model allied with a linear anisotropic elastic stress model. MASTRAPP (multizone adaptive scheme for simulation of transport and phase change phenomena) is a numerical model designed for modelling material-processing operations, and includes all the physics and techniques discussed in §4. The thermal conditions were roughly simulated, and care was taken to maintain the exact shape of the experimentally grown necked crystal throughout the numerical simulation.

Figure 11 presents a sample snapshot of the stress calculations in the crystal at six different crystal heights. The colours correspond to the values of the maximum of the resolved shear stresses on the 12 different slip systems in the InP lattice. The stresses range from 5 MPa to 15 MPa, and the maximum stress at any given instant occurs at a distance of 7 mm from the crystal/melt interface, on the edge of the crystal. This distance corresponds to the height of the encapsulation used in the furnace, and is consistent with previous works (Zou *et al* 1996), confirming that the maximum stress in the growing crystal occurs on the edge of the crystal, just as it emerges from under the encapsulation and is exposed to the ambient gas. Figure 12 shows the variation of the maximum excess shear stress experienced by elements on the surface of the crystal through the entire growth history.

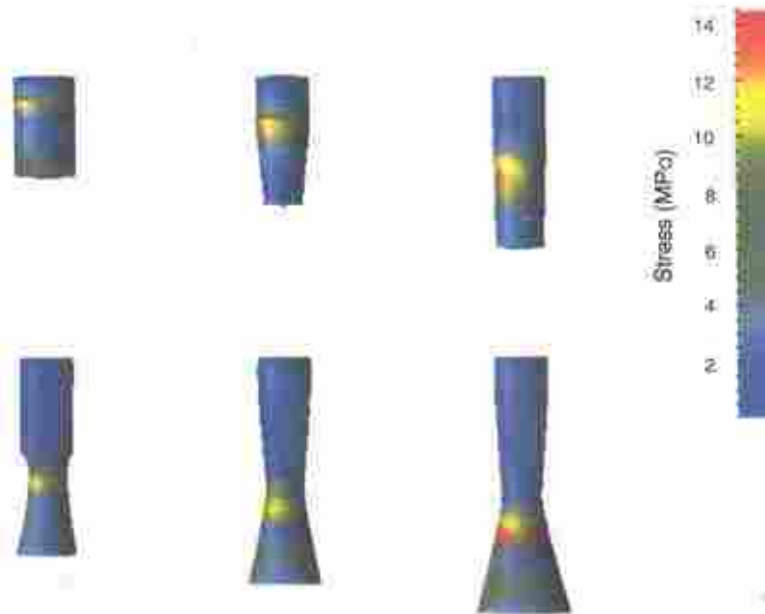
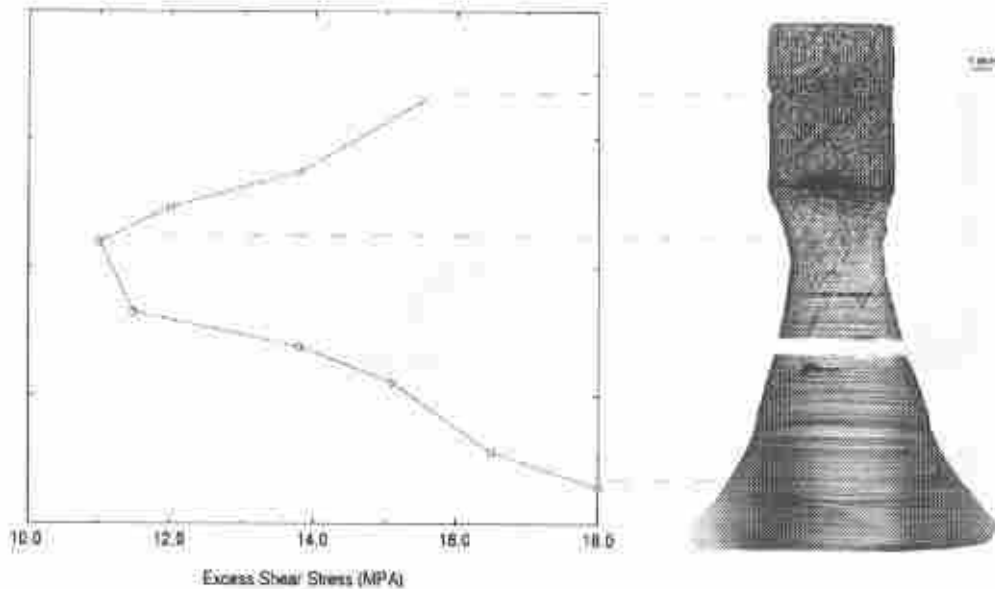


Figure 11. Simulated stress distribution at different stages of growth of the crystal.

As noted above, an element on the edge of the crystal experiences this maximum shear stress at that point in growth history when it just emerges from the encapsulant. It can be seen that the magnitude of the stress in figure 12 scales with the diameter of crystal. This has implications and the observations are detailed above – the presence of a dislocation-free region, below lines  $A_1$ ,  $A_2$  figure 10c, followed by the reappearance of dislocations, when the crystal exceeds a critical diameter of around 15mm. The stresses in the regions above  $A_1$ ,  $A_2$  are sufficient for the glide and multiplication of preexisting dislocations in the seed. Since these dislocations glide only along  $\{111\}$  planes, the preexisting dislocations in the seed are active only in the regions above lines  $A_1$  and  $A_2$  and cannot enter the region below them.

Consequently, the region below these lines remains free of dislocations. This scenario changes once the crystal reaches a larger diameter, where the stress as per figure 12 attains high values. One can tentatively propose that the high stress is responsible for the nucleation of new dislocations in this area. The exact reason for the nucleation of new dislocations is unknown – seven probable reasons are suggested at the beginning of § 5.1. It is well-established that twinning is primarily related to oscillations in the shape of the crystal/melt interface. The occurrence of twinning in the growing crystal, once it reaches a critical diameter may be linked to changes in the shape of the crystal melt/interface, which is intimately linked to the flow pattern in the melt. Figure 13a gives a detailed view of the flow pattern in the melt, when the crystal diameter is 16 mm. The thermal conductivity of the crystal is very high compared to the encapsulant and the crystal basically acts as a medium for the transfer of heat from the melt to the ambient. Since the diameter of the crystal is relatively narrow, the recirculatory flow under the crystal is very strong and consequently bifurcates into two cells below the crystal.



**Figure 12.** Plot showing the maximum shear stress experienced by particles on the surface of the crystal during their entire growth history.

Figure 13b presents a similar view of the flow pattern when the diameter of the crystal is 40mm. Since the crystal here is of a larger diameter, the flow is not concentrated entirely under the crystal. Here the flow bifurcates horizontally into two distinct cells, with a shear layer present between them. The change in the structure of the flow necessarily entails a change in the structure of the melt/crystal interface, which is tracked in figure 14 at different instants of the growth history of the crystals. One can see that the structure of the interface undergoes a large variation. The crystal/melt interface becomes more convex towards the melt from a diameter of 9 mm to a diameter of 26 mm, and then starts becoming less convex, henceforth. In the above simulation, the deflection of the interface is rather slight because of the low macroscopic flow parameters, such as Reynolds number or Grashof number, of the flow used here. In a real system, the effects due to the above detailed change in the structure of the flow will be much larger. Thus, with the aid of simulation, tentative reasons have been advanced for the occurrence of twinning and dislocations, once the crystal has exceeded a certain critical diameter.

## 7. Conclusion

A brief review of the modelling issues and formulations for transport phenomena and defect modelling has been presented. Rapid advances in semiconductor technology have led to the demand for single crystals of new novel semiconductor materials and also large and defect-free crystals of traditional materials like Si, GaAs etc. The process of achieving this poses considerable technological challenges, and numerical modelling using high-

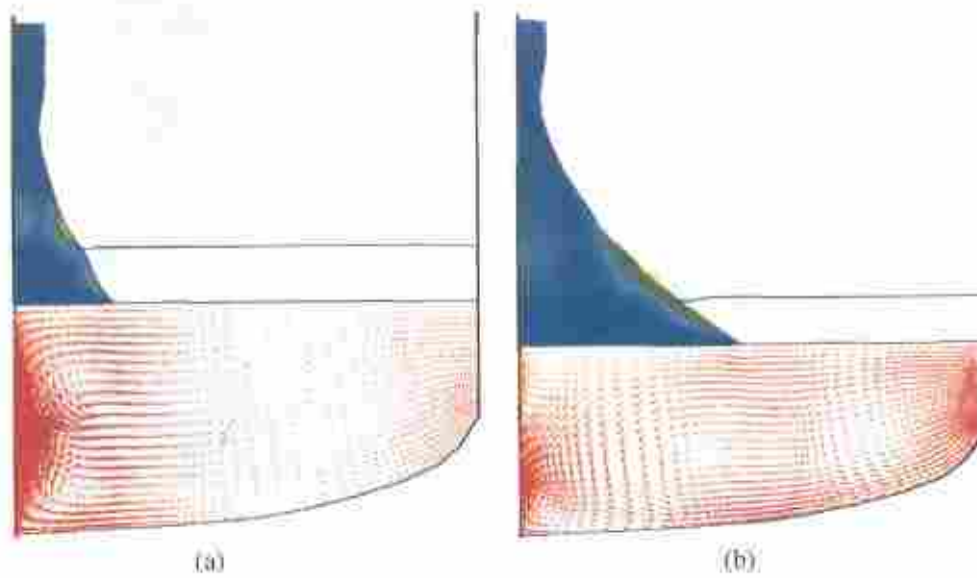


Figure 13. Plots to illustrate changes in flow structure during the course of the growth. Detailed view of the flow pattern in the melt when the crystal diameter is 16 mm (a) and 40 mm (b).

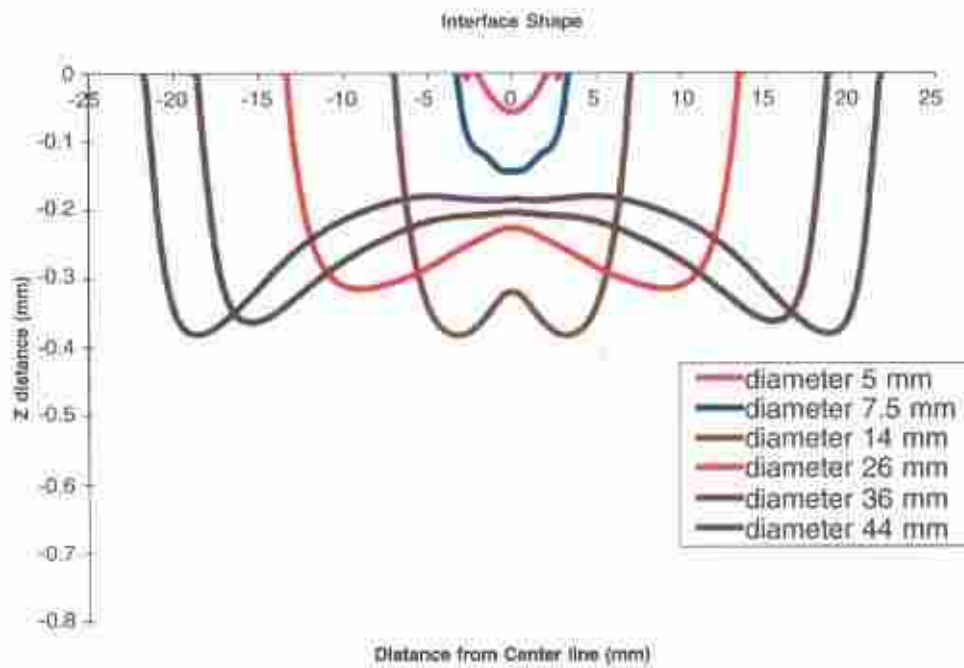


Figure 14. Shape of the solidification interface at different stages of the growth process. (Note that the scale on z-axis is greatly exaggerated.)

speed computers has emerged as a powerful tool. Modelling of traditional crystal growth processes like Czochralski or Bridgman require a number of formulations involving various transport phenomena, special schemes for treating complicated boundary conditions involving free surfaces and solidification interfaces, and powerful grid generation techniques, modelling of defects formed during the growth process being of crucial importance. In III-V and II-VI semiconductors, the primary defects are line defects called dislocations formed as a result of plastic deformation, under the influence of thermal stresses due to thermal gradients. Two specific models of increasing degree of complexity have been presented to describe this phenomenon. Defect modelling, though still immature, is very important and is the subject of intense on-going research. Due to various roadblocks in modelling the process such as our limited understanding of the physics of certain phenomena, lack of models suitable to describe them, and the diverse time scales needed to solve such problems, a full-fledged, real-time model involving all the physics, and simulating the entire growth process from beginning to end, remains a challenging task.

## References

- Alexander H 1986 Dislocations in covalent crystals. In *Dislocations in solids* (ed.), F R N Nabarro (Amsterdam: North-Holland) vol. 7, pp 113-234
- Alexander H, Haasen P 1968 Dislocations in the diamond structure In *solid state physics* (eds) F Seitz, D Turnbull, H Ehrenreich (New York & London: Academic Press) vol. 22, pp 28-158
- Anselmo A, Prasad V, Koziol J, Gupta K P 1993 Numerical and experimental study of a solid pellet feed continuous Czochralski growth process for silicon single crystals. *J. Cryst. Growth* 131: 247-264
- Atherton L, Derby J J, Brown R A 1987 Radiative heat exchange in Czochralski crystal growth. *J. Cryst. Growth* 84: 57-78
- Bardsley W, Frank F C, Green G, Hurle D T J 1974 Meniscus in Czochralski growth. *J. Cryst. Growth* 23: 341-344
- Batchelor G K 1967 *An introduction to fluid mechanics* (London: Cambridge University Press) ch. 1
- Brice J C, King G D 1966, Effect of arsenic pressure on dislocation densities in melt-grown gallium arsenide. *Nature* (London) 209: 1346
- Brown R A 1988 Theory of transport processes in single-crystal growth from the melt. *AIChE J.* 34: 881-911
- Chaudari A R, Patel J R, Rubin L G 1962 Velocities and densities of dislocations in germanium and other semiconductor crystals. *J. Appl. Phys.* 22: 2736
- Chen R T, Holmes D E 1983 Dislocation studies in 3-inch diameter liquid encapsulated Czochralski GaAs. *J. Cryst. Growth* 61: 111
- Chen T C, Wu H C, Weng C I 1997 The effect of interface shape on anisotropic thermal stress of bulk single crystals during Czochralski growth. *J. Cryst. Growth* 173: 367-379.
- Czochralski J 1917 Ein neues Verfahren zur Messung der Kristallisations-Geschwindigkeit der Metalle. *Z. Phys. Chem.* 92: 219-221
- Dash W C 1958 Dislocation free silicon crystals. In *Growth and perfection of crystals* (ed.) R M Doremus, B W Roberts, D. Turnbull (New York: Wiley)
- George A, Rabier J 1987 Dislocations and plasticity in semiconductors. I. Dislocation-structures and dynamics. *Rev. Phys. Appl.* 22: 941-966
- Hurle D T J, Cockayne B 1994 Czochralski growth. In *Handbook of crystal growth* (ed.) D T J Hurle (New York: North-Holland) vol. 2a, pp 99-211
- Jones A D W 1983 An experimental-model of the flow in Czochralski growth. *J. Cryst. Growth* 61: 235-244

- Jordan A S, Caruso R, Von Neida A R 1980 A thermoelastic analysis of dislocation generation in pulled GaAs crystals. *Bell Syst. Tech. J.* 59: 593-637
- Jordan A S, Von Neida A R, Caruso R 1986 The theoretical and experimental fundamentals of decreasing dislocations in melt grown GaAs and InP. *J. Cryst. Growth* 79: 243-262
- Jordan A S, Mounberg E M, Clemans J E 1993 Thermal-stress theory of dislocation reduction in the vertical gradient freeze (VGF) growth of GaAs and InP. *J. Cryst. Growth* 128: 444-450
- Kobayashi N 1978 Computational simulation of melt flow during Czochralski growth. *J. Cryst. Growth* 43: 357-363
- Kobayashi S, Miyahara S, Fujiwara T, Kubo T, Fujiwara H 1991 Turbulent heat-transfer through the melt in silicon Czochralski growth. *J. Cryst. Growth* 109: 149-154
- Kopetsch H 1989 Numerical simulation of the Czochralski bulk flow of silicon on a domain confined by a moving crystal interface and curved melt-gas meniscus. *PhysicoChem. Hydrodyn.* 11: 357-375
- Lambropoulos J C, Wu C H 1996 Mechanics of shaped crystal growth from the melt. *J. Mater. Res.* 11: 2163-2176
- Langlois W E 1981 Convection in Czochralski growth melt. *PhysicoChem. Hydrodyn.* 2: 245-261
- Maroudas D, Brown R A 1991 On the prediction of dislocation formation in semiconductor crystal grown from the melt - Analysis of the Haasen model for plastic deformation dynamics. *J. Cryst. Growth* 108: 399-415
- Miyazaki N, Kuroda Y 1998 Dislocation density simulations for bulk single crystal growth process. *Metals Mater., Korea* 4: 883-890
- Miyazaki N, Kuroda Y 1999 Finite element analysis of dislocation density during bulk crystal growth (effect of doping atoms in InP single crystal growth). *J. Cryst. Growth* 196: 62-66
- Miyazaki N, Okuyama S 1998 Development of finite element computer program for dislocation density of bulk semiconductor single crystals during Czochralski growth. *J. Cryst. Growth* 183: 81-88
- Miyazaki N, Hagiwara S, Munakata T 1990 Elastic-constant matrix required for thermal-stress analysis of bulk single-crystals during czochralski growth. *J. Cryst. Growth* 106: 149-156
- Moosbrugger J C 1995 Continuum slip viscoplasticity with the Haasen constitutive model - Application to single-crystal inelasticity. *Int. J. Plasticity* 11: 799-826
- Moosbrugger J C, Levy A 1995 Constitutive modeling for CdTe single-crystals. *Metal. Mater. Trans. A* 26: 2687-2697
- Nabarro F R N, Basinski Z S, Holt D B 1964 The plasticity of pure single crystals. *Adv. Phys.* 13: 193-323
- Nunes E M, Naraghi M H N, Zhang H, Prasad V 1996 Combined radiative-convection modeling for materials processes: Application to crystal growth. *Proc. 31<sup>st</sup> Natl. Heat Transfer Conference* (New York: ASME) HTD-vol. 323, pp 27-37
- Parsey J M Jr, Naitishi Y, Lagowski J, Gatos H C 1982 Bridgman-type apparatus for the study of growth-property relationships - Arsenic vapor pressure GaAs property relationship. *J. Electrochem. Soc.* 129: 388-393
- Patel V C, Rodi W, Scheuerer G 1985 Turbulence models for near wall and low Reynolds number flows. *AIAA J.* 23: 1308-1319
- Rabier J, George A 1987 Dislocations and plasticity in semiconductors. 2. The relation between dislocation dynamics and plastic-deformation. *Rev. Phys. Appl.* 22: 1327-1351
- Schvezov C, Samarasekera I V, Weinberg F 1989 Temperature and stress field calculations in indium phosphide during LEC growth. *J. Cryst. Growth* 97: 146-151
- Shinoyama S, Uemura C, Yamamoto A, Tshno S 1980 Growth of dislocation free undoped InP crystals. *Jpn. J. Appl. Phys.* 19: L331-L334
- Siethoff H 1992 The plasticity of elemental and compound semiconductors. *Semiconductors and Semimetals* 37: 143-187
- Sumino K, Yonenaga I 1993 Dislocation dynamics and mechanical behavior of elemental and compound semiconductors. *Phys. Stat. Sol. (a)* 138: 573-581

- Surek T, Chalmers B 1975 Direction of growth of surface of a crystal in contact with its melt. *J. Cryst. Growth* 29: 1–11.
- Taylor G I 1934 The mechanism of plastic deformation of crystals. Part I Theoretical. *Proc. R. Soc.* 145: 362–387
- Teal G K, Little J B 1950 Growth of germanium single crystals. *Phys. Rev.* 78: 647
- Thakur S, Wright J, Shyy W, Liu J, Ouyang H, Vu T 1996 Development of pressure-based composite multigrid methods for complex fluid flows. *Prog. Aerosp. Sci.* 32: 313–375
- Tsai C T 1991 On the finite-element modeling of dislocation dynamics during semiconductor-crystal growth. *J. Cryst. Growth* 113: 499–507
- Tsai C T, Gulluoglu A N, Hertley C S 1993 A crystallographic methodology for modeling dislocation dynamics in GaAs crystals grown from the melt. *J. Appl. Phys.* 73: 1650–1656
- Voekl J 1994 Stress in the cooling crystal. In *Handbook of crystal growth* (ed.) D T J Hurle (New York: North-Holland) vol. 2a, pp 823–874
- Voekl J, Mueller G, Blum W, 1987 Analysis of generation and movement of dislocations in InP by a study of deformation-behavior. *J. Cryst. Growth* 83: 383–390
- Yakhot V, Orszag S A 1986 Renormalization group analysis of turbulence. I. Basic theory. *J. Sci. Comput.* 1: 1–51
- Zhang H, Prasad V 1995 A multizone adaptive process model for low and high pressure crystal growth. *J. Cryst. Growth* 155: 47–65
- Zhang H, Mollemi M K 1995 A multizone adaptive grid generation technique for simulation of moving and free boundary value problems. *Numer. Heat Transfer* B27: 255–276
- Zhang H, Prasad V, Bliss D 1995 Transport phenomena in high pressure crystal growth systems for III-V compounds *J. Cryst. Growth* 169: 250–260
- Zhang H, Prasad V, Mollemi M K 1996 A numerical algorithm using multizone grid generation for multiphase transport processes with moving and free boundaries. *Numer. Heat Transfer* B29: 399–421.
- Zhang T, Ladeinde F, Zhang H, Prasad V 1996 A comparison of turbulence models for natural convection in enclosures: applications to crystal growth processes. *ASME Proc. 31<sup>st</sup> National Heat Transfer Conf.* (ASME) HTD-vol. 323, pp 17–26
- Zhang H, Zheng L, Prasad V, Larson D J Jr 1998a Local and global simulations of Bridgman and Czochralski crystal growth. *J. Heat Transfer* 120: 865–873
- Zhang H, Zheng L, Prasad V, Larson D J Jr 1998b Diameter controlled Czochralski growth of silicon crystal. *J. Heat Transfer* 120: 874–882
- Zhang T, Wang G X, Zhang H, Ladeinde F, Prasad V 1999 Turbulent transport of oxygen in the Czochralski growth of large silicon melt. *J. Cryst. Growth* 198: 141–146.
- Zhao J Y, Bliss D F, Dudley M, Huang X R, Raghobhachar B, Bryant G, Lancto R, Zhang H, Prasad V 2001 Assessment of the necking process as a strategy for dislocation reduction in magnetic liquid encapsulated Czochralski crystal growth of sulfur-doped InP. *J. Cryst. Growth* (to be published)
- Zou Y F, Zhang H, Prasad V 1996 Dynamics of melt-crystal interface and thermal stresses in Czochralski crystal growth processes *J. Cryst. Growth* 166: 476–482